

Fluid dynamic insights into virus deposition and transport in the deep lung

Aranyak Chakravarty^a, Mahesh V. Panchagnula^b, Neelesh A. Patankar^{c,*}

^a*School of Nuclear Studies & Application, Jadavpur University, Kolkata, India*

^b*Department of Applied Mechanics, Indian Institute of Technology Madras, Chennai, India*

^c*Department of Mechanical Engineering, Northwestern University, Evanston, IL, USA*

Abstract

The primary mode of respiratory virus transmission is by means of virus-laden aerosols. The aerosols are inhaled into the respiratory tract and deposited in the mucosa, where the virus may interact with the epithelial tissue causing infection. Transport of virus within the respiratory tract, and its clearance from the lungs, is extremely important to limit the chance of an infection. In this work, these phenomena are mathematically modelled using a coupled model of aerosol transport and virus transport within a Weibel-like idealisation of the lung geometry. The analysis is carried out in a dimensionless form and the results are presented in terms of various non-dimensional parameters. It is observed that the main factor determining virus transport and clearance from the lungs is the location of deposition of the virus-laden aerosols. Viruses deposited in the upper respiratory tract are cleared out of the lung relatively faster by means of mucociliary clearance. Viruses deposited in the deep lung persist much longer due to weak diffusive transport and the absence of mucociliary clearance. Deep lung deposition of viruses, thus, increases the likelihood of the viruses infecting an individual. Deep lung deposition is observed to take place for a specific range of aerosol sizes. Slower breathing and deep breaths are observed to promote deep lung deposition. Slower breathing and faster mucus clearance are also observed to enhance virus clearance from the upper respiratory tract. It is further observed that virus clearance from the deep lung can only be enhanced by increasing virus diffusivity. This enhancement is, however, not substantial. It, thus, becomes imperative to eliminate deep lung deposition of the viruses. Larger exposure durations are also observed to result in substantially larger virus concentrations, which increases the clearance time and as such, the risk of infection. Hence, limiting the exposure time also becomes essential to reduce the chance of an infection.

Keywords: aerosol transport, virus deposition, mucociliary clearance, virus transport, mathematical modelling

1. Introduction

Respiratory viruses (e.g. SARS-CoV-2) are transmitted mainly through virus-laden droplets and aerosols [1]. These are formed within the respiratory tract of an infected individual, which in turn can be directly inhaled or expelled into the environment by various mechanisms (talking, sneezing, coughing, and even normal exhalation) and subsequently inhaled by other individuals. Once inhaled, the droplets/aerosols travel along the respiratory tract following breathing dynamics and are deposited in the respiratory mucosa through different mechanisms [2]. The mucosa provides a certain level of protection for the respiratory tract from the deposited viruses [3]. As such, inhalation and deposition of virus-laden droplets/aerosols does not always lead to infection of the individual. Even when an individual does get infected, they may remain asymptomatic or exhibit mild symptoms in certain cases, while major health complications such as pneumonia may occur in other cases. Such variation in symptoms could be a manifestation of the interaction of the viruses with the mucosa. It can also depend on the transport of the deposited viruses within the respiratory tract. No definite answer is currently available. The present article attempts to computationally analyse the deposition and

*Corresponding author

Email address: n-patankar@northwestern.edu (Neelesh A. Patankar)

transport of viruses within the respiratory tract by using a coupled analysis of aerosol and virus transport within the lungs.

It is known that the transport of aerosols in the respiratory system is governed by the combined effects of unsteady convective air flow, gravitational settling, and diffusion of aerosols within air. The inhaled aerosols travel along the respiratory tract during which they may deposit in the mucosa due to different physical mechanisms. The principal deposition mechanisms are diffusion, sedimentation, and inertial impaction [2, 4, 5]. While inertial impaction remains significant in the upper airways, sedimentation and diffusion are the dominant mechanisms in the deeper airways [4]. The extent of influence of these mechanisms is determined by the size, shape, and distribution of the aerosols as well as the breathing pattern (tidal volume, breathing frequency, air flow rate etc) and the morphology of the respiratory tract [5].

Computational modelling of aerosol transport and deposition in the respiratory tract has been carried out using different techniques [5]. Both Eulerian and Lagrangian approaches have been used for such modelling. Some of these models consider localised regions of the lung for analysis. Such localised models may range from a single airway to bifurcating channels and even a branching network comprising a few lung generations [6, 7, 8]. At the other extreme are *whole lung* models that consider the lung to be a network of interconnected branching channels with varying dimensions. Such *whole lung* models include semi-empirical regional compartment models [9], one-dimensional *trumpet* models [10, 11], and various mechanistic models [5]. A common requirement in all *whole lung* models is an assumption of the lung morphometry. The most widely used lung morphometric model is the Weibel model [12], which is based upon detailed morphometric data of the branching lung geometry. Other models include the ones proposed by Yeh and Schaum [13] and Horsfield and Cumming [14].

The respiratory mucosa acts as a barrier between the airway lumen and the epithelial tissue lining the respiratory tract (see Fig. 1). The aerosols deposited in the mucosa do not directly come into contact with the epithelial cells. The mucosa comprises of two liquid sub-layers - the mucus layer lining the airway lumen and the periciliary layer beneath it [15]. The epithelium is also lined with cilia that beats metachronously within the periciliary layer [16]. This beating mechanism displaces the mucus from the distal regions of the lung towards the top of the trachea, where it is either swallowed or expectorated. Such mucociliary transport provides a natural defense of the lungs against foreign particles in general and viruses in particular. It is, thus, essential to consider the mucociliary transport while analysing virus transport in the lungs. Mathematical models of virus spread in respiratory tracts generally take into account infection kinetics that describes the temporal evolution of virus spread. A large volume of work has been carried out in evaluating virus spread and localisation using these models through various approaches [17, 18, 19]. However, only a few have taken into consideration the impact of virus diffusion in the mucus and mucociliary clearance on virus spread in the respiratory tract. Quirouette et al. [3] evaluated the spread and localisation of Influenza A virus in the human respiratory tract using one such model. They observed that virus diffusion has negligible effect as compared to mucociliary transport, which effectively clears the lungs off the virus. Infection peaks and resolves faster in the upper respiratory tract than the lower tract. However, they considered only a portion of the upper respiratory tract in their analysis and not the whole lung.

To our knowledge, none of the mathematical models for virus spread have considered coupled aerosol (in airways) and virus (in mucosa) transport models, although these processes occur simultaneously within the lung. The present article reports the development of a coupled mathematical model of aerosol and virus transport within a Weibel-like one-dimensional model of the human lung. Aerosol deposition is calculated using appropriate empirical models. It is also assumed that airflow within the lungs and aerosol transport are one-way coupled – air flow is not affected by aerosols but aerosols are carried by flowing air. This assumption is valid for low aerosol concentrations [6]. This eliminates the need for solving airflow equations explicitly. The mathematical model is reduced to a dimensionless form using suitable scaling parameters and is used to study the impact of pertinent dimensionless parameters on virus transport within the lung.

2. Mathematical Modelling

2.1. Idealisation of the lung geometry

The lung geometry considered in this analysis is an idealisation of the physiological network of airways and alveoli that is encountered in a real lung. Physiological investigations have estimated that a real human lung can be subdivided into approximately 24 generations (0 – 23) based on bifurcation of the bronchioles,

with distinct length and cross-sectional areas of each generation [12]. The number of bronchioles in each generation is estimated to be 2^N , where N is the generation number. Further, investigations have revealed that airways are alveolated from generation 17 onwards with increasing alveolation as one moves deeper down the generations.

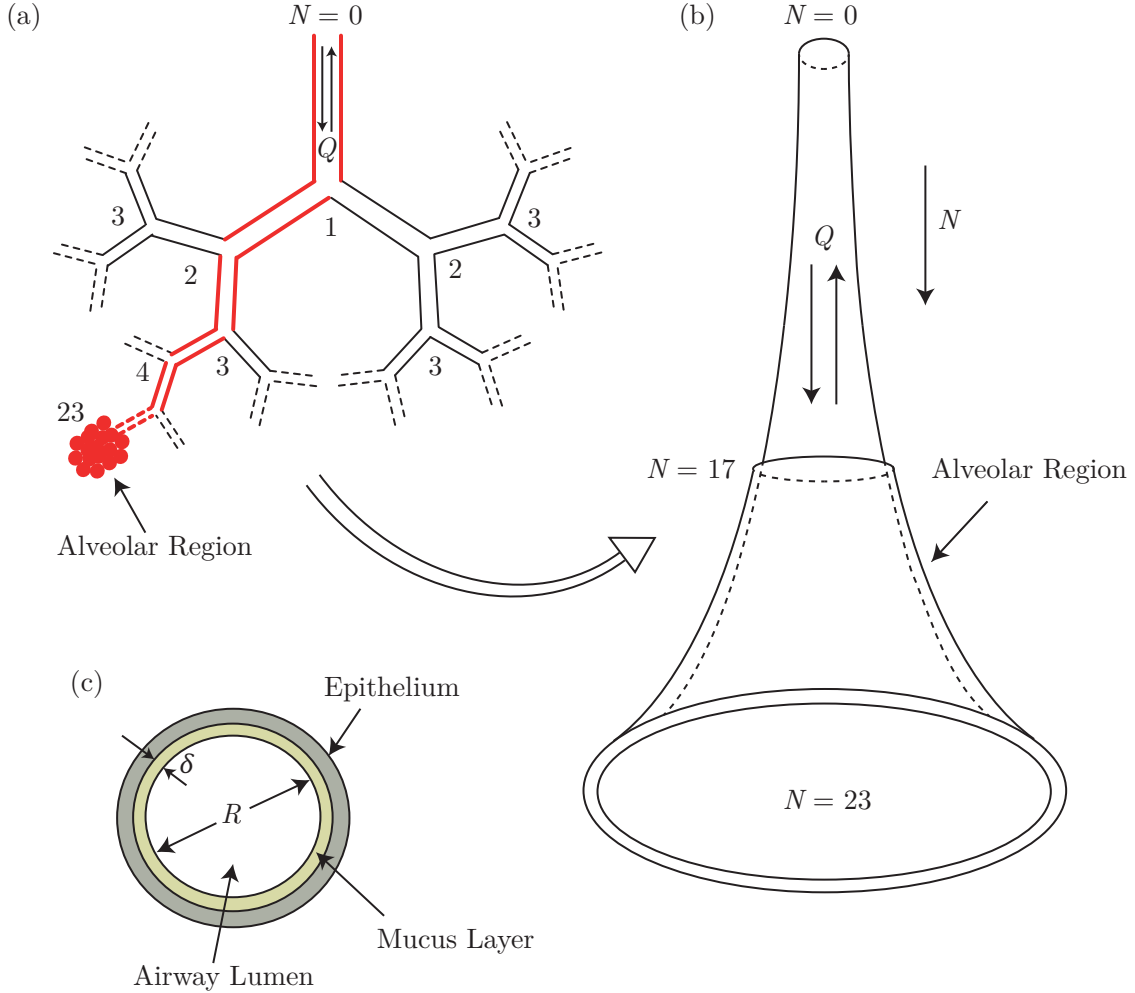


Figure 1: Schematic illustration of (a) the network of airways and alveoli representing the dichotomous branching structure of a human lung (b) one-dimensional *trumpet* model that is used in the present analysis to approximate the dichotomous network structure of a human lung (c) Cross-sectional view of the *trumpet* model showing the arrangement of the airway lumen, mucus layer and epithelial lining in the lungs.

Figure 1 schematically represents the modelled system of airways and alveoli. The dichotomous branching network encountered in a human lung (Fig. 1a) is approximated by a one-dimensional *trumpet* model (Fig. 1b). While this model cannot account for the effects of heterogeneities in the lung, it is still a tractable model for the whole lung that can capture the key trends of interest.

The airway is modelled as a continuous one-dimensional channel of variable cross-sectional area and length divided into 24 generations ($N = 0 - 23$). The length (L) and cross-sectional area (A) of each generation (N) is calculated using a power-law function as

$$L_N = L_0 \alpha^N, \quad (1)$$

$$A_N = A_0 (2\beta)^N, \quad (2)$$

where L_0 and A_0 represents the length and cross-sectional area at $N = 0$, respectively (see Table 1 for

Table 1: Parameters used in modelling the lung geometry

L_0	0.12 m [12]	α	0.73
A_0	0.000317m ² [12]	β	0.71
R_0	$\sqrt{A_0/\pi}$	ζ	0.9
δ_0	10 μ m [16]	ε	0.87
$A_{m,0}$	$2\pi R_0\delta_0$		
$V_{m,0}$	-5 mm/min [16]		

Table 2: Fractions of alveolated airways in different generations [20]

Lung Generation (N)	Fraction of alveolated area (γ)
0-16	0
17	0.0011
18	0.0041
19	0.0135
20	0.0509
21	0.1168
22	0.2712
23	0.5424

magnitudes). The quantities α and β are defined as the length-change and area-change factors, respectively. The magnitudes of α and β are selected (see Table 1) such that the computed length and area matches the experimentally observed magnitudes as closely as possible [12].

Alveolation of the airways is considered from generation 17 onwards as in a real human lung . Table 2 lists the fractions of the airway area that is assumed to be alveolated in different generations. The modelled system of airways and alveoli is also assumed to be lined by a thin mucus layer that separates the airway lumen from the epithelium. The mucus layer has a uniform advective motion from the deeper generations towards the 0th generation that is a consequence of muco-ciliary transport arising due to ciliary beating mechanism. Thickness of the mucus layer as well as the advective motion of the mucus layer is assumed to be temporally invariant in this analysis [16]. Thickness (δ) and area of mucus layer (A_m), and the advective mucus velocity due to mucociliary transport (V_m) at different lung generations are also estimated using a power-law function as

$$\delta_N = \delta_0 \zeta^N, \quad (3)$$

$$A_{m,N} = A_{m,0} (2\sqrt{\beta}\zeta)^N, \quad (4)$$

$$V_{m,N} = V_{m,0} \varepsilon^N, \text{ for } N < 18, \quad (5)$$

$$= 0, \text{ for } N \geq 18,$$

where δ_0 , $A_{m,0}$, and $V_{m,0}$ are the mucus thickness, area, and velocity at $N = 0$, respectively (see Table 1 for magnitudes). The magnitudes of ζ and ε used in this analysis are also listed in Table 1 and are chosen based on experimental data [16]. Note that the mucus velocity due to mucociliary transport is considered only till $N = 18$ (Eq. 5) due to absence of any appreciable mucociliary transport in the deep lung [21, 22].

2.2. Aerosol transport

The 1D transport equation for aerosol particles in the idealised lung geometry is given below

$$\frac{\partial(A_N c_{ae,N})}{\partial t} + \frac{\partial(Q c_{ae,N})}{\partial x} = \frac{\partial}{\partial x} (A_N D_{ae} \frac{\partial c_{ae,N}}{\partial x}) - L_{dep} c_{ae}, \quad (6)$$

where c_{ae} represents the aerosol concentration, Q represents the volume flow rate of air in breathing, and D_{ae} represents the diffusivity of aerosols in air. The term L_{dep} accounts for the aerosols deposited in the airway mucus. This equation is based on the *trumpet* model proposed by Taulbee & Yu [10] and later used

by various authors to study different aspects of aerosol deposition in the lung [11, 23, 24]. The transport equation is formulated based on the assumption that the aerosol particles are monodispersed, do not undergo coagulation, and are decoupled from airflow in the lungs. It is also assumed that external forces (such as electrical and magnetic forces) do not have any influence on the aerosol particle dynamics. It is further assumed that there is no additional source of aerosols present within the lungs and the aerosols are either deposited in the airway mucus or washed out of the airways.

Eq. 6 is presented in terms of airway length (x), while the lung model adopted is in terms of lung generation number (N). As such, Eq. 6 needs to be converted to a more appropriate form in terms of N . This requires an additional mathematical relation (Eq. 7) connecting airway length x and the lung generation number (N) given by

$$\frac{\partial N}{\partial x} = -\frac{1 - \alpha}{L_0 \alpha \ln(\alpha) \alpha^N}. \quad (7)$$

Converting Eq.6 using Eqs. 7 and 2, we get

$$A_0(2\beta)^N \frac{\partial c_{ae,N}}{\partial t} = \frac{\partial N}{\partial x} \frac{\partial}{\partial N} \left[\left(A_0(2\beta)^N D_{ae} \frac{\partial N}{\partial x} \frac{\partial c_{ae,N}}{\partial N} \right) - \left(Q_{max} q(t) c_{ae,N} \right) \right] - L_{dep} c_{ae}, \quad (8)$$

where $q(t)$ represents the temporal function accounting for airflow variation such that $Q = Q_{max} q(t)$. Eq. 8 is reduced to its dimensionless form by multiplying and dividing Eq. 8 with $\left(\frac{L_0}{A_0 D_{ae}} \right)$ and $\left(-\frac{\alpha \ln(\alpha)}{1 - \alpha} \right)$, respectively, and using the following variables

$$\tau = \frac{t}{T_b}, \phi_{ae,N} = \frac{c_{ae,N}}{c_{ae,0}}, T_a = \frac{L_0 A_0}{|Q_{max}|}, St_a = \frac{T_a}{T_b}, |Pe_{ae,max}| = \frac{|Q_{max}| L_0}{A_0 D_{ae}}, D_{ae} = \frac{k_B T C_s}{6\pi \mu_{air} r_{ae}}, \quad (9)$$

where Pe_{ae} and St_a are the Peclet number for the aerosols and Strouhal number for the airways, respectively. ϕ_{ae} and τ denotes the dimensionless aerosol concentration and time, respectively, while the quantities T_a and T_b represents the convective airflow time-scale and breathing time-scale, respectively. The expression of D_{ae} is based on the Stokes-Einstein relation [6], where C_s represents the Cunningham slip correction, T represents the ambient temperature, μ_{air} denotes air viscosity, and r_{ae} denotes the aerosol size.

The dimensionless equation, thus, obtained is used to analyse aerosol transport in the present study and is given by

$$|Pe_{ae,max}| St_a (2\alpha\beta)^N \frac{\partial(\phi_{ae,N})}{\partial \tau} = \frac{\partial}{\partial N} \left[\left(\left(\frac{2\beta}{\alpha} \right)^N \left(\frac{1 - \alpha}{\alpha \ln(\alpha)} \right)^2 \frac{\partial \phi_{ae,N}}{\partial N} \right) + \left(|Pe_{ae,max}| q(t) \left(\frac{1 - \alpha}{\alpha \ln(\alpha)} \right) \phi_{ae,N} \right) \right] - L'_{dep} \phi_{ae}, \quad (10)$$

where L'_{dep} represents the dimensionless form of the aerosol deposition (L_{dep}) and is expressed as

$$L'_{dep} = L_{dep} \frac{L_0^2}{A_0 D_{ae}} \alpha^N. \quad (11)$$

2.3. Aerosol deposition models

The major mechanisms of aerosol deposition in the lungs have been identified in the literature as diffusion, sedimentation and impaction of the aerosols in the airways, as well as diffusion and sedimentation in the alveoli [5, 11]. Different empirical models have been used to estimate the different depositions. However, these models need to be converted into a more appropriate form for use in the present analysis.

The probability of aerosol deposition in the airways by diffusion (P_d), sedimentation (P_s) and impaction (P_i) can be expressed following Yeh & Schaum [13] as

$$\frac{c_{ae,0} - c_{ae}}{c_{ae,0}} = P_d + P_s + P_i - P_d P_s - P_d P_i - P_s P_i - P_d P_s P_i \quad (12)$$

On algebraic manipulation, Eq. 12 can be re-written as

$$\begin{aligned} \frac{c_{ae}}{c_{ae,0}} &= (1 - P_d)(1 - P_s)(1 - P_i) = \left(\sum C_{d,n} e^{-k_{d,n}x} \right) (C_s e^{-k_s x}) (C_i e^{-k_i x}) \\ &\implies c_{ae} = c_{ae,0} \sum \left[C_{d,n} C_s C_i e^{-(k_{d,n} + k_s + k_i)x} \right] \end{aligned} \quad (13)$$

Taking the derivative of Eq. 13 with respect to x , we obtain -

$$\frac{dc_{ae}}{dx} = -c_{ae,0} \sum \left[(k_{d,n} + k_s + k_i) C_{d,n} C_s C_i e^{-(k_{d,n} + k_s + k_i)x} \right] = -(k_{d,n} + k_s + k_i) C_{ae} \quad (14)$$

Equation 14 represents the aerosol deposition flux in the airways. It is further converted to a dimensionally relevant form for use in the transport equation (Eq. 8) as follows -

$$\frac{D(Ac_{ae})}{Dt} \simeq Av \frac{dc_{ae}}{dx} = -Av(k_{d,n} + k_s + k_i) C_{ae} = L_{dep} c_{ae} \implies L_{dep} = Av(k_{d,n} + k_s + k_i) \quad (15)$$

The empirical relations for the different deposition mechanisms are converted to a form relevant to Eq. 15 and then reduced to their dimensionless forms for use in the final transport equation (Eq. 10).

2.3.1. Diffusional deposition in the airways

The probability of diffusional deposition of the aerosols in the airways is expressed following Yeh & Schaum [13] as

$$P_d = 1 - 0.819e^{-7.315x} - 0.0976e^{-44.61x} - 0.0325e^{-114x} \quad (16)$$

On linearisation of the above equation following Eq. 13, we obtain -

$$k_{d,1} = 7.315 \frac{D_{ae}}{2R_N^2 v_N}, k_{d,2} = 44.61 \frac{D_{ae}}{2R_N^2 v_N}, k_{d,3} = 114 \frac{D_{ae}}{2R_N^2 v_N} \quad (17)$$

and

$$k_d = k_{d,1} + k_{d,2} + k_{d,3} = (7.315 + 44.61 + 114) \frac{D_{ae}}{2R_N^2 v_N} \quad (18)$$

where, R_N and v_N denotes the airway radius and airflow velocity of a respective lung generation, respectively. Using this, aerosol deposition in the airways due to aerosol diffusion is estimated as

$$L_{dep,d} = v_N A_{N,T} k_d = v_N \pi R_N^2 2^N (7.315 + 44.61 + 114) \frac{D_{ae}}{2R_N^2 v_N} \quad (19)$$

Conversion of Eq. 19 to its dimensionless form gives us the following expression for dimensionless diffusional deposition of the aerosols in the airways -

$$L'_{dep,d} = L_{dep,d} \frac{L_0^2}{A_0 D_{ae}} \alpha^N = \left(\frac{L_0}{R_0} \right)^2 (2\alpha)^N (3.66 + 22.305 + 57) \quad (20)$$

2.3.2. Sedimentation deposition in the airways

The probability of deposition of the aerosols due to sedimentation in the airways is expressed following Yeh & Schaum [13] as

$$P_s = 1 - \exp \left[- \left(\frac{4gC_s \rho_{ae} r_{ae}^2 \cos(\psi_N)}{9\pi \mu_{air} R_N v_N} x \right) \right] \quad (21)$$

where, ρ_{ae} , g and ψ represents aerosol density, gravitational acceleration and airway orientation angle considering horizontal as 90° , respectively. Linearising the above equation using the approach followed in Eq.13, we obtain -

$$k_s = \frac{4gC_s\rho_p r_p^2 \cos(\psi_N)}{9\pi\mu_{air}R_N v_N} \quad (22)$$

Aerosol deposition in the airways due to sedimentation can, then, be estimated as -

$$\begin{aligned} L_{dep,s} &= v_N A_{N,T} k_s = v_N (\pi R_N^2 2^N) \frac{4gC_s\rho_p r_p^2 \cos(\psi_N)}{9\pi\mu_{air}R_N v_N} \\ &= \frac{4}{9} \frac{R_N g C_s \rho_p r_p^2 \cos(\psi_N)}{\pi\mu_{air}} 2^N \end{aligned} \quad (23)$$

Conversion of the dimensional deposition ($L_{dep,s}$) to its dimensionless form gives us the following expression for dimensionless sedimentation deposition in the airways -

$$L'_{dep,s} = L_{dep,s} \frac{L_0^2}{A_0 D_{ae}} \alpha^N = \frac{8}{3} \left(\frac{L_0}{R_0} \right)^2 (2\alpha\sqrt{\beta})^N S_g \cos(\psi_N) \quad (24)$$

where, S_g is defined as the sedimentation parameter and expressed as

$$S_g = \frac{R_0 \rho_p r_p^3 g}{k_B T} \quad (25)$$

2.3.3. Impact deposition in the airways

The probability of deposition due to impaction of the aerosols in the airways is given by Yeh & Schaum [13] as

$$P_i = 1 - f_i(\theta, St) \quad (26)$$

where, θ denotes the branching angle of the airways and St denotes the Stokes number ($= \frac{C_s \rho_p r_p^2 v_N}{9\mu_{air} R_N}$). The function $f_i(\theta, St)$ is expressed as follows -

$$\begin{aligned} f_i(\theta, St) &= \frac{2}{\pi} \cos^{-1}(\theta \cdot St) - \frac{1}{\pi} \sin \left[2 \cos^{-1}(\theta \cdot St) \right] \text{ for } \theta \cdot St < 1 \text{ (Inhalation)} \\ &= 1 \text{ for } \theta \cdot St \geq 1 \text{ (Exhalation)} \end{aligned} \quad (27)$$

The expression of P_i is not in a form that can be directly linearised. As such, certain mathematical treatments need to be carried out in order to estimate the impact deposition. Loss of aerosols in one generation of the lungs can be determined based on the aerosol concentrations before and after the lung generation. Mathematically, this can be expressed as

$$\begin{aligned} \text{Loss in a generation} &= \frac{C_{bef} - C_{aft}}{C_{bef}} = 1 - f_i(\theta, St) \\ \implies \frac{C_{aft}}{C_{bef}} &= f_i(\theta, St) \end{aligned} \quad (28)$$

In terms of lung generations, the above expression can be re-written as

$$C_N = f_i^N(\theta, St) C_0 \quad (29)$$

Differentiating with respect to generation number, we obtain -

$$\frac{dC_N}{dN} = C_0 \ln(f_i^N(\theta, St)) f_i^N(\theta, St) = \ln(f_i^N(\theta, St)) C_N \quad (30)$$

Converting the above derivative to a derivative in terms of x , we get -

$$\begin{aligned}\frac{dC(x)}{dx} &= -(-\ln(f_i^N(\theta, St)))\frac{dN}{dx}C(x) \\ \implies k_i &= (-\ln(f_i^N(\theta, St)))\frac{dN}{dx}\end{aligned}\quad (31)$$

The impact deposition is estimated using the above expression as

$$L_{dep,i} = v_N A_{N,T} k_i = v_N \pi R_N^2 2^N (-\ln(f_i^N(\theta, St)))\frac{dN}{dx}\quad (32)$$

The dimensionless form of the impact deposition is obtained following a similar approach as in Sections 2.3.1 and 2.3.2. The dimensionless impact deposition, thus, obtained is expressed as

$$L'_{dep,i} = L_{dep,i} \frac{L_0^2}{A_0 D_{ae}} \alpha^N = |Pe_{ae,max}| q(t) \ln(f_i^N(\theta, St)) \frac{(1-\alpha)}{\alpha \ln(\alpha)}\quad (33)$$

2.3.4. Diffusional deposition in the alveoli

Diffusional deposition of the aerosols in the alveoli is estimated using the following dimensionless expression -

$$L'_{dep,d,alv} = \gamma_N \eta_{d,alv} |Pe_{ae,max}| q(t) \left(\frac{1-\alpha}{-\alpha \ln(\alpha)} \right)\quad (34)$$

where, γ_N denotes the fraction of alveolated area in the corresponding generation (see Table 2) and $\eta_{d,alv}$ denotes the diffusional deposition efficiency in the alveoli. $\eta_{d,alv}$ is expressed as [11]

$$\eta_{d,alv} = 1 - \frac{6}{\pi^2} \sum \frac{1}{k^2} \exp \left[-\frac{4k^2 t D_{ae}}{d_{eq}^2} \right]\quad (35)$$

2.3.5. Sedimentation deposition in the alveoli

Deposition of the inhaled aerosols due to their sedimentation in the alveoli are estimated using the following dimensionless expression -

$$L'_{dep,s,alv} = \gamma_N \eta_{s,alv} |Pe_{ae,max}| q(t) \left(\frac{1-\alpha}{-\alpha \ln(\alpha)} \right)\quad (36)$$

where, γ_N and $\eta_{s,alv}$ denotes the fraction of alveolated area in the corresponding generation (see Table 2) and sedimentation deposition efficiency in the alveoli, respectively. $\eta_{s,alv}$ is expressed as [11]

$$\eta_{s,alv} = \left[1 + \min \left(\frac{d_s}{d_{eq}}, 1 \right) \right]^2 \left[1 - 0.5 \min \left(\frac{d_s}{d_{eq}}, 1 \right) \right]^2 - 1\quad (37)$$

2.4. Virus transport

The corresponding 1D transport equation for the virus particles in the airway mucus is expressed as

$$\frac{\partial(A_{m,N} c_{vi,N})}{\partial t} + \frac{\partial(Q_m c_{vi,N})}{\partial x} = \frac{\partial}{\partial x} (A_{m,N} D_{vi} \frac{\partial c_{vi,N}}{\partial x}) + Source\quad (38)$$

where, c_{vi} denotes the virus concentration in the airway mucus, Q_m represents the volume flow rate of mucociliary clearance and D_{vi} denotes the diffusivity of viruses in the mucus layer.

The virus-laden aerosols deposited in the airway mucus serve as the only source of virus in the lungs. The *Source* term in Eq. 38 is, therefore, equivalent in magnitude to the deposition term in Eq. 6 ($L_{dep,ae}$) times the *viral load* (ϕ_l). Mathematically, this is expressed as -

$$Source = L_{dep,ae} \phi_l\quad (39)$$

where, ϕ_l is defined as the quantity of virus contained by the aerosols per unit quantity of the aerosol. Equation 38 is converted to a form in terms of N using Eqs. 7 and 4 in a similar manner as in Section 2.2 as follows -

$$A_{m,0}(2\zeta\sqrt{\beta})^N \frac{\partial x}{\partial N} \frac{\partial c_{vi,N}}{\partial t} = \frac{\partial}{\partial N} \left[\left(A_{m,0}(2\zeta\sqrt{\beta})^N D_{vi} \frac{\partial c_{vi,N}}{\partial N} \right) - \left(Q_{m,0}(2\varepsilon\zeta\sqrt{\beta})^N c_{vi,N} \right) \right] + (\phi_l L_{dep} c_{ae}) \frac{\partial x}{\partial N} \quad (40)$$

The above equation is further reduced by multiplying and dividing by $\left(\frac{L_0}{A_{m,0} D_{vi}} \right)$ and $\left(-\frac{\alpha \ln(\alpha)}{1-\alpha} \right)$, respectively. The reduced equation is expressed as

$$\frac{L_0 |V_{m,0}|}{D_{vi}} (2\alpha\zeta\sqrt{\beta})^N \frac{T_m}{T_b} \frac{\partial c_{vi,N}}{\partial t} = \frac{\partial}{\partial N} \left[\left(\left(\frac{2\zeta\sqrt{\beta}}{\alpha} \right)^N \left(\frac{1-\alpha}{\alpha \ln(\alpha)} \right)^2 \frac{\partial c_{vi,N}}{\partial N} \right) - \left(\frac{L_0 |V_{m,0}|}{D_{vi}} (2\varepsilon\zeta\sqrt{\beta})^N c_{vi,N} \right) \right] + \left(\phi_l L'_{dep} \frac{A_0 D_{ae}}{L_0^2 \alpha^N} \phi_{ae} c_{ae,0} \frac{L_0^2 \alpha^N}{A_{m,0} D_{vi}} \right) \quad (41)$$

The following parameters are utilised to achieve the dimensionless form of the virus transport equation in the airway mucus given by Eq. 43.

$$\tau = \frac{t}{T_b}, \phi_{vi,N} = \frac{c_{vi,N}}{c_{vi,0}}, c_{vi,0} = \phi_l c_{ae,0} \frac{A_0}{A_{m,0}}, T_m = \frac{L_0}{|V_{m,0}|}, St_m = \frac{T_m}{T_b}, |Pe_{vi,max}| = \frac{|V_{m,0}| L_0}{D_{vi}}, D_{vi} = \frac{k_B T}{6\pi \mu_m r_{vi}} \quad (42)$$

$$|Pe_{vi,max}| (2\alpha\zeta\sqrt{\beta})^N St_m \frac{\partial \phi_{vi,N}}{\partial \tau} = \frac{\partial}{\partial N} \left[\left(\left(\frac{2\zeta\sqrt{\beta}}{\alpha} \right)^N \left(\frac{1-\alpha}{\alpha \ln(\alpha)} \right)^2 \frac{\partial \phi_{vi,N}}{\partial N} \right) - \left(|Pe_{vi,max}| (2\varepsilon\zeta\sqrt{\beta})^N \phi_{vi,N} \right) \right] + \left(L'_{dep} \frac{D_{ae}}{D_{vi}} \phi_{ae} \right) \quad (43)$$

where, ϕ_{vi} , Pe_{vi} and St_m represents the dimensionless virus concentration, Peclet number for viruses and Strouhal number for the mucus layer, respectively. T_m denotes the time-scale for mucociliary transport. Virus diffusivity (D_{vi}) is estimated using the Stokes-Einstein relation where μ_m represents mucus viscosity and r_{vi} represents virus size.

2.5. Initial and boundary conditions

The entire lung is assumed to have zero concentration of aerosols as well as virus i.e. $\phi_{ae} = \phi_{vi} = 0$ at all generations initially ($\tau = 0$). Boundary conditions need to be specified at the two extremes of the lung i.e. at $N = 0$ and $N = 23$ for both aerosol and virus transport equations. These are summarised below.

$$N = 0: \phi_{ae} = 1, \tau \leq \tau_{inhalation} \text{ (Inhalation)} \\ \phi_{ae} = 0, \tau > \tau_{inhalation} \text{ (Inhalation)}$$

$$\frac{\partial(\text{Total flux of aerosols})}{\partial N} = 0 \text{ (Exhalation)}$$

$$\frac{\partial(\text{Total flux of virus})}{\partial N} = 0 \text{ (Inhalation/Exhalation)}$$

$$N = 23: \text{Total flux of aerosols} = 0 \text{ (Inhalation/Exhalation)} \\ \text{Total flux of virus} = 0 \text{ (Inhalation/Exhalation)}$$

2.6. Implementation of the model and validation

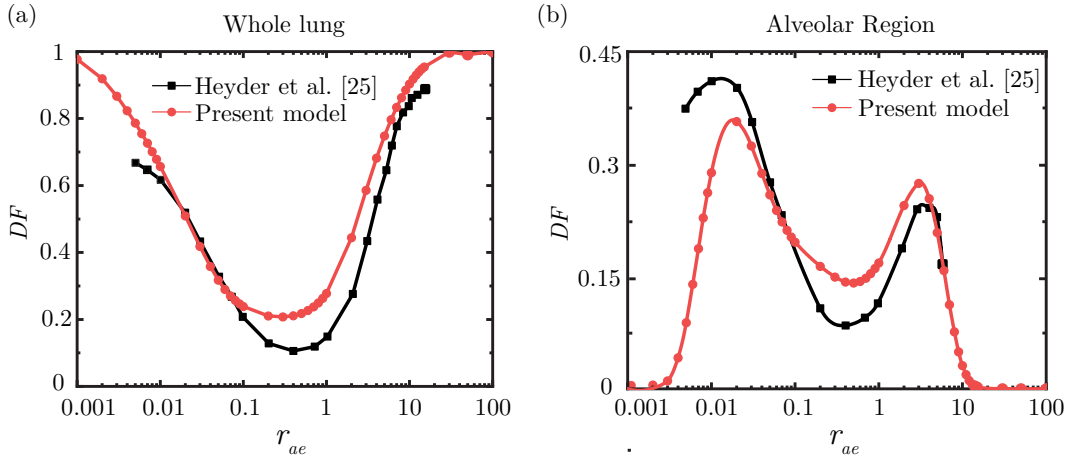


Figure 2: Comparison of the calculated deposition fraction (DF) of inhaled aerosols for (a) the whole lung and (b) the alveolar region with the experimental results obtained by Heyder et al. [25] for different aerosol sizes (r_{ae})

The mathematical model discussed in Sections 2.2-2.4 is implemented for computational analysis using MATLAB[®]. The governing transport equations are discretised following the finite-difference technique with a first-order upwind and central-difference scheme used for the advective and diffusive terms, respectively. The temporal term is discretised using explicit forward differencing.

The implemented mathematical model is validated with respect to aerosol deposition within the lung - the most crucial aspect determining virus transport. Aerosol depositions predicted using the computational model are compared with the experimental data of Heyder et al. [25] with respect to deposition in the whole lung as well as deposition specifically in the alveolar region of the lung. The results are shown in Fig. 2. It can be observed that the computed aerosol deposition is in quite good agreement with the experimentally determined data.

3. Results

The results discussed in Sections 3.1 and 3.2 have been obtained using the following dimensionless parameters - $Pe_{ae,max} = 2.85 \times 10^{10}$, $Pe_{vi,max} = 4.56 \times 10^7$, $St_a = 0.0095$, $St_m = 359.7122$, and $\tau_{exp} = 5$. Parametric studies for these parameters (Sections 3.3.1-3.3.5) have been carried out by varying the specific parameter only, while the other base parameters remain unchanged. It is assumed while obtaining the results that temporal airflow variation ($q(t)$) during breathing follows a sinusoidal function.

3.1. Aerosol transport and deposition in the airways

Figure 3a represents the distribution of aerosol concentration (ϕ_{ae}) within the adopted lung geometry at various instances of a breathing cycle. Two different situations are shown - with and without considering aerosol deposition in the respiratory mucosa in order to highlight the impact of deposition on aerosol transport within the lung. It can be observed that, in either case, the aerosol concentration front gradually progresses into the deeper regions of the lung during inhalation part of the breathing cycle and reaches its extreme position at the end of inhalation. The reverse happens during exhalation with a substantial volume of the inhaled aerosols getting washed out of the lung. A comparison between the two cases, however, indicate substantial differences with respect to the location of the concentration front as well as its magnitude. The differences can be attributed to deposition of the aerosols in the airway mucus. It can be observed that the concentration fronts nearly overlap each other at the peak of inhalation, with the front for the deposition case located marginally behind that of the non-deposition case. With progress in the breathing cycle, more aerosols get deposited in the airways and the alveoli and hence, the gap between the two cases widen. As expected, the residual concentration of aerosols at the end of a breathing cycle is substantially less when

deposition is considered. The deposition of aerosols in the respiratory mucosa is shown in Fig. 3c with respect to the lung generations for the case when deposition is considered.

The impact of deposition on aerosol transport is also evident from a comparison of the aerosol washout curves between the two cases, as shown in Fig. 3b. The washout curves represent the temporal variation of aerosol concentration at the 0^{th} generation of the lung. Aerosol concentration increases during inhalation, while it reduces during exhalation, for the duration of aerosol exposure i.e. up to $\tau = 5$. Beyond that, the residual aerosols are quickly washed out of the lung. It can be observed that the nature of the washout curves are similar to that observed for gaseous transport in the lung. However, washout of the aerosols take place at a much faster rate as compared to the gases, which can be primarily attributed to the much smaller diffusivity of the aerosols in air.

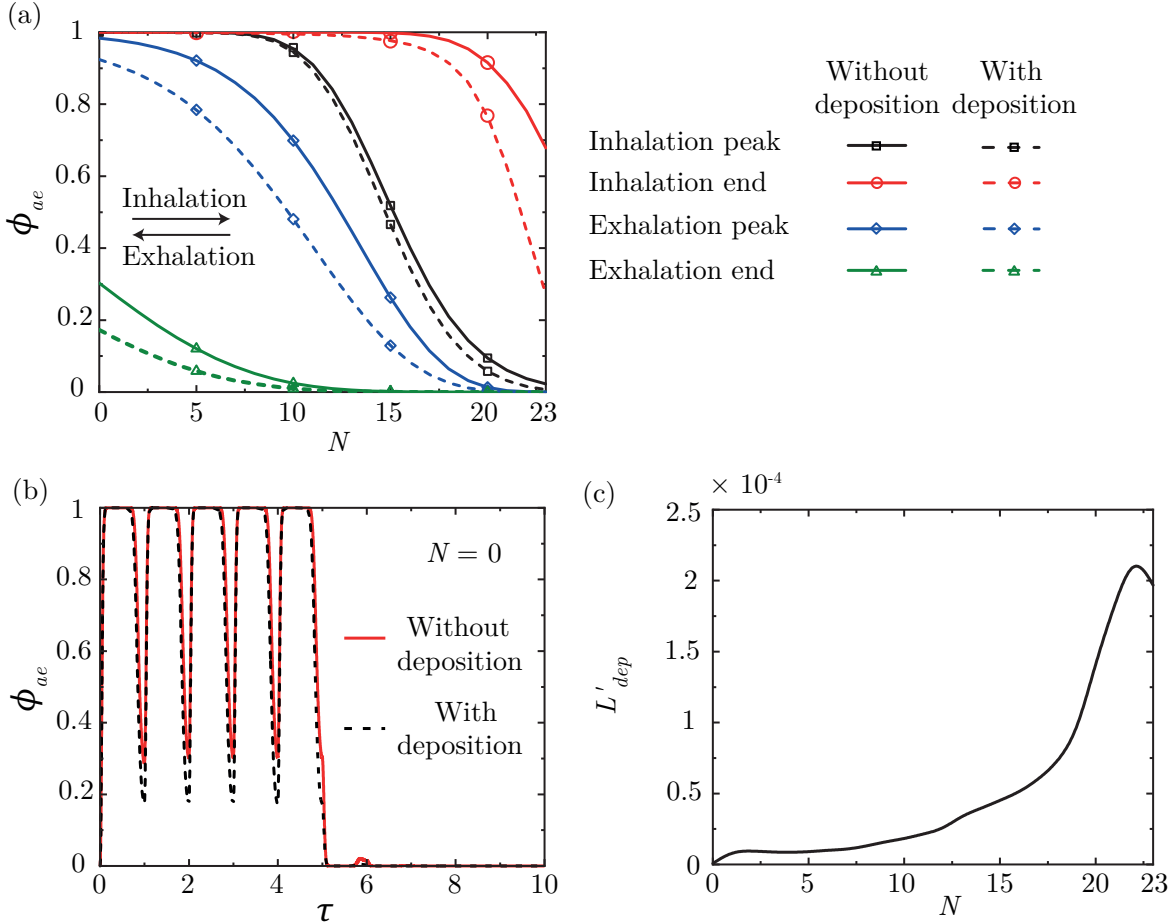


Figure 3: (a) Aerosol concentration with lung generations at different instances of a breathing cycle for two different cases - with and without aerosol deposition in the respiratory mucosa (b) Temporal change in aerosol concentration at the 0^{th} generation of the lung with and without aerosol deposition (c) Aerosol deposition within the lung for the case when deposition is considered. The results shown are for $Pe_{ae,max} = 2.85 \times 10^{10}$ and $St_a = 0.0095$.

3.2. Virus transport in the airway mucus

The only source of virus in the respiratory mucosa is through the deposition of virus-laden aerosols in the mucosa. Viruses deposited in the mucosa diffuse through the mucus layer and are also transported upstream through the airways due to muco-ciliary transport. Deposition of virus-laden aerosols and the advective-diffusive transport of viruses in the mucosa are, thus, coupled processes with aerosol deposition dominating over virus transport when aerosol inhalation is taking place. As such, virus concentration in the mucus (ϕ_{vi}) at the end of aerosol exposure ($\tau = 5$), as shown in Fig. 4a, qualitatively follows the aerosol deposition pattern (see Fig. 3c). However, virus transport - which occurs simultaneously with aerosol

deposition - results in the deposited viruses being transported away from the initial deposition location even before deposition is complete. This results in minor qualitative deviations between the virus concentration curve at $\tau = 5$ and the aerosol deposition curve. The deviation is especially evident around $N = 18$ as a result of the change in virus transport mechanism about this generation (see Section 2.1).

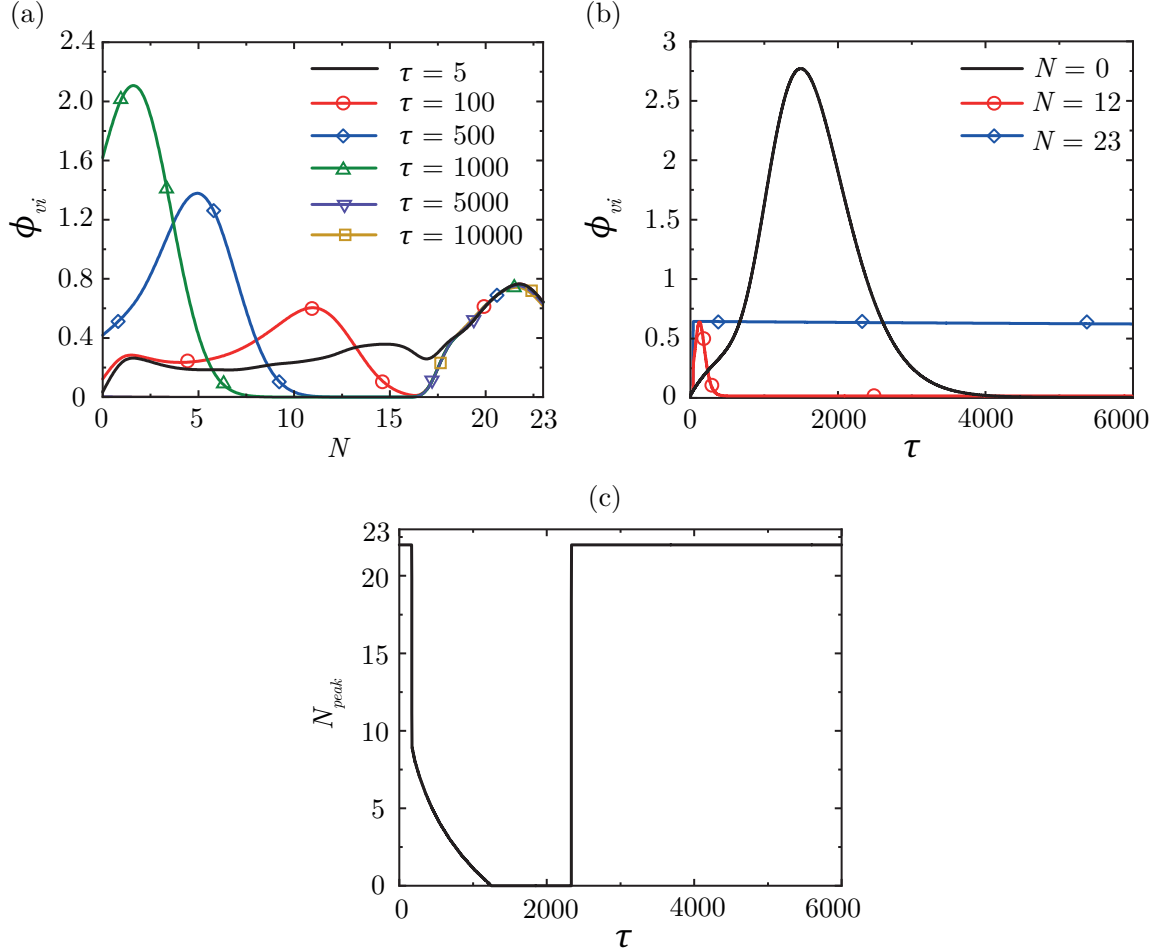


Figure 4: (a) Virus concentrations within the lung at different time instances (b) Temporal change in virus concentration at $N = 0, 12, 23$ (c) Change in location of peak virus concentration within the lung with time. The results shown are for $Pe_{ae} = 2.85 \times 10^{10}$, $St_a = 0.0095$, $Pe_{vi} = 4.56 \times 10^7$, $St_m = 359.7122$, $\tau_{exp} = 5$.

Viruses deposited in generation 18 onwards are transported purely by diffusion of the viruses due to absence of muco-ciliary transport, while the viruses deposited from generation 0 to 18 are transported through the combined action of muco-ciliary transport and diffusion of the viruses. Muco-ciliary transport is, however, much stronger as compared to the diffusive transport of the viruses within the mucus. The difference in the strength of transport results in a sharp change in virus concentration as observed at $N = 18$.

Viruses deposited before $N = 18$ are transported towards the 0^{th} generation and ultimately cleared out of the lung primarily as a result of the muco-ciliary transport. It is evident from Fig. 4a that the viruses - being transported from the deeper to the upper generations - result in accumulation in the upper generations leading to larger ϕ_{vi} in the upper generations (due to smaller volume) as time progresses, before clearing out of the lung. The temporal change in virus concentration at the 0^{th} generation in Fig. 4b also corroborates this.

Viruses deposited beyond generation 18 are not subjected to this clearance and virus concentration in this region, therefore, undergoes very slow change as can be expected in a situation with very weak diffusive transport. As such, viruses deposited in this region of the lung persists for a much longer time as compared to those deposited before generation 18. This is clearly evident from Figs. 4a-b. The location of the peak

virus concentration undergoes change with time, as can be seen from Fig. 4c. Initially, the peak location remains in generation 22 for a certain period of time before advective transport results in the concentration increasing in the upper generations. The peak location, as such, shifts to the upper generations. The peak location once again shifts to the deeper generation after the advective clearance is complete.

A longer residence time of the viruses within the lung provides the viruses more time to infect an individual. The probability of a serious infection, thus, rises as the virus residence time becomes longer. The probability of such serious infections increase drastically in the deep lung, where the respiratory mucosa becomes thin enough to allow the viruses to come in close contact with the blood vessels. A longer residence time in the deep lung, thus, allows the viruses to pass on to the blood stream from the alveoli and potentially to other parts of the body by blood circulation. It is, thus, of immense importance to understand the various situations under which the viruses can be deposited in the deep lung and persist there. These situations are identified through a parametric analysis of the relevant parameters in Section 3.3.

3.3. Impact of different pertinent parameters

3.3.1. Aerosol Peclet number

Peclet number for the aerosols (Pe_{ae}) is defined as the ratio of advective transport of aerosols due to airflow and diffusive transport of the aerosols in air (see Eq. 9). The range of Pe_{ae} considered in this analysis is selected based on physiologically realistic air flow rate in the lungs and inhaled aerosol sizes.

A larger Pe_{ae} indicates a greater dominance of advective transport of aerosols with respect to diffusive transport of aerosols and vice-versa. Increase in Pe_{ae} , therefore, leads to the aerosols reaching deeper parts of the lung. As a consequence, a larger volume of aerosols are deposited in the deeper generations of the lung with increase in Pe_{ae} . This is clearly evident from Fig. 5a. This trend is, however, observed to be reversed i.e. aerosol deposition shifts towards the upper generations, when $Pe_{ae,max}$ is increased beyond 1.59×10^9 . At $Pe_{ae,max} = 3.07 \times 10^{11}$, maximum deposition is observed to occur in the first few generations with reducing deposition towards the deeper generations and almost no deposition in the deep lung (beyond $N = 18$). Similar observations have been made in previous investigations as well [26]. The reason is due to a larger contribution of impact deposition of the aerosols in the earlier generations at such high Pe_{ae} . Diffusional and sedimentation deposition dominates over impact deposition at relatively lower Pe_{ae} .

Figures 5(b-c) shows the virus concentration in the mucosa for different $Pe_{ae,max}$ at the end of aerosol exposure ($\tau = 5$). Wide variation in ϕ_{vi} for different $Pe_{ae,max}$ makes it difficult to present all the plots in a single figure and as such, the plots are subdivided into two separate figures. It can be observed from both these plots that ϕ_{vi} at the end of exposure ($\tau = 5$) qualitatively follows the aerosol deposition patterns (Fig. 5a). While ϕ_{vi} remains substantial in the deep lung for $Pe_{ae,max} \leq 9.03 \times 10^{10}$, only negligible ϕ_{vi} is observed in the deep lung for $Pe_{ae,max} > 9.03 \times 10^{10}$. Interestingly, washout of the viruses from the lung does not undergo any significant temporal change with variation in $Pe_{ae,max}$, as evident from Fig. 5d. However, the initial location of virus deposition within the lung is observed to have an important impact on its washout, as discussed in Section 3.2. Viruses deposited before $N = 18$ gets washed out quickly due to the stronger muco-ciliary clearance. Viruses deposited beyond $N = 18$, however, gets transported much slowly due to the weak diffusive transport of viruses in that region. Viruses deposited at very large $Pe_{ae,max}$ ($\sim 3.07 \times 10^{11}$) are, therefore, washed out of the lungs relatively quickly since majority of the deposition takes place before $N = 18$. At lower $Pe_{ae,max}$, however, a substantial amount of the deposited viruses continue to persist in the deep lung (beyond $N = 18$) even though muco-ciliary clearance washes out the viruses from the upper generations. The persistence of viruses in the deep lung is evident from the distribution of ϕ_{vi} within the lung at $\tau = 10000$ in Fig. 3e.

3.3.2. Airway Strouhal number

Strouhal number for the airways (St_a) is defined in this analysis as the ratio of convective airflow time scale to the breathing time scale. Physiological considerations result in St_a varying between 0.001 and 0.1. The same is taken as the range of study in this analysis.

An increase in St_a can be the result of an increase in the convective airflow time scale (which translates to a reduced airflow velocity) or a reduction in T_b , and vice-versa. In either case, this results in decreasing amount of aerosols being inhaled and the concentration front progression into the lung progressively decreasing. Consequently, smaller amounts of aerosol are deposited in the mucus and the deposition also tends to shift towards the upper airways with increase in St_a . The change in deposition with variation in St_a , as shown in

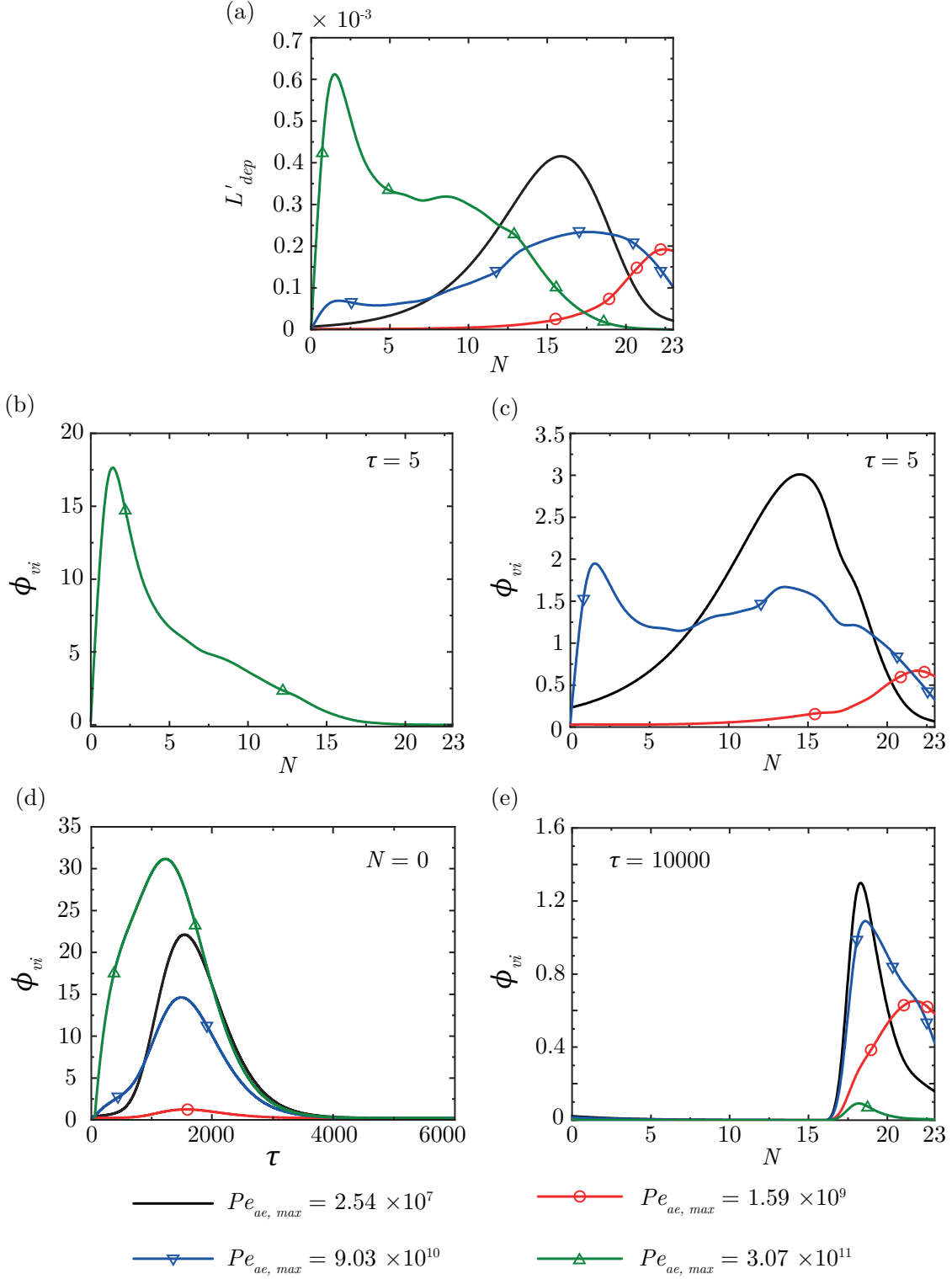


Figure 5: (a) Aerosol deposition within the lung for different Pe_{ae} (b) Virus concentration within the lung at $\tau = 5$ for $Pe_{ae, max} = 3.07 \times 10^{11}$ (c) Virus concentration within the lung at $\tau = 5$ for $Pe_{ae, max} = 2.54 \times 10^7$, 1.59×10^9 and 9.03×10^{10} (d) Temporal change in virus concentration at $N = 0$ for different $Pe_{ae, max}$ (e) Virus concentration within the lung at $\tau = 10000$ for different $Pe_{ae, max}$

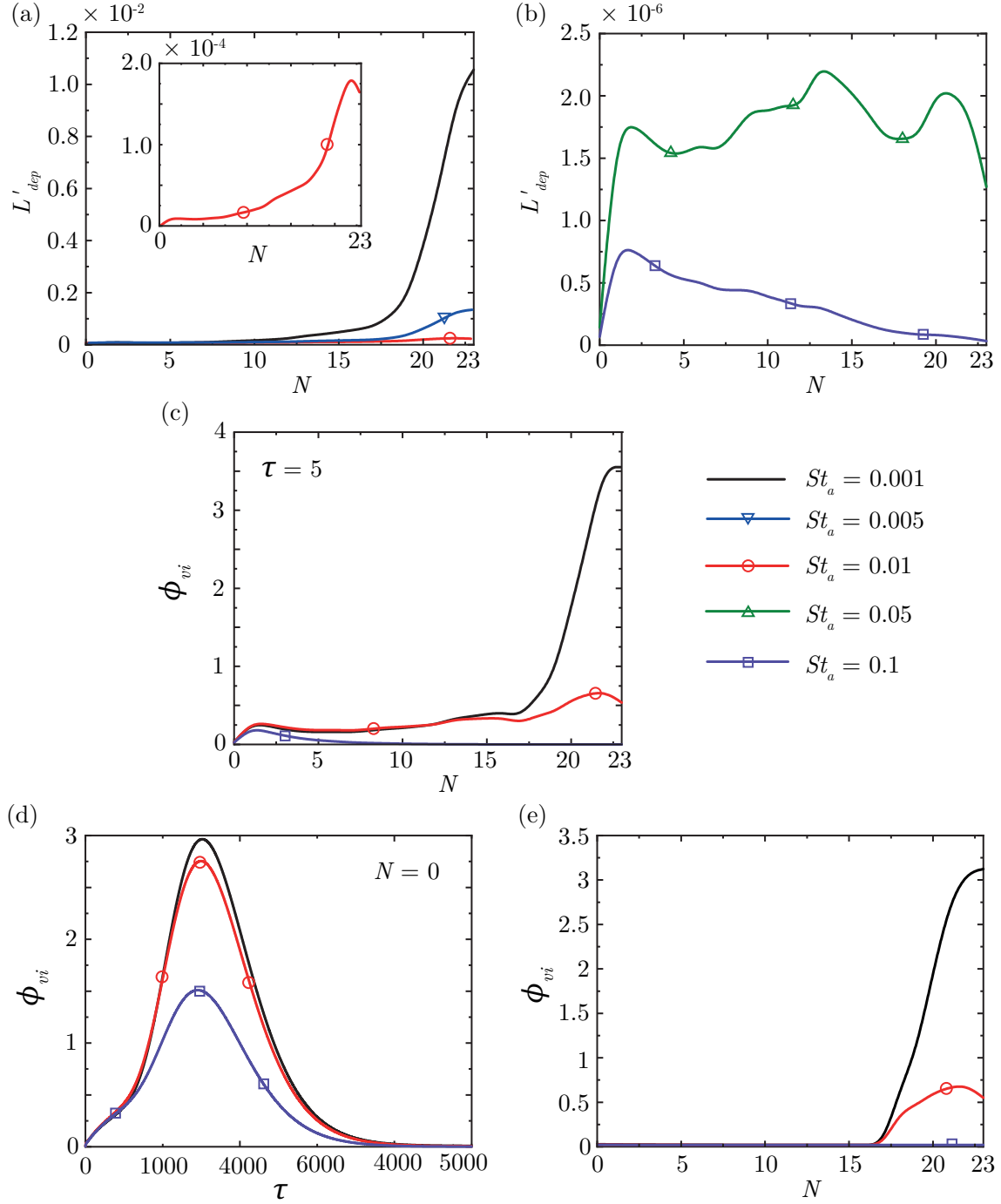


Figure 6: (a-b) Aerosol deposition within the lung for different St_a (c) Virus concentration within the lung for different St_a at $\tau = 5$ and $\tau = 10000$ (d) Temporal change in virus concentration at $N = 0$ for different St_a (e) Virus concentration within the lung for different St_a at $\tau = 10000$

Fig. 6a-b, adequately highlights this. Reducing aerosol deposition with increase in St_a results in decreasing virus concentration as well. This is evident from a comparison of virus concentration for different St_a at the end of exposure ($\tau = 5$) in Fig. 6c. Qualitative nature of the curves remain similar to the deposition patterns shown in Fig. 6a-b. It is also observed that ϕ_{vi} remains substantial in the deep lung when $St_a \leq 0.01$, but becomes negligible at $St_a \geq 0.05$.

Any change in St_a , however, do not affect the mucus clearance rate from the lung or diffusivity of the virus in the mucosa. Virus washout from the lung, therefore, remains unaffected when St_a is changing, as shown from the temporal change of virus concentration at $N = 0$ in Fig. 6d. Persistence of viruses in the deep lung is, as such, observed for the situations where deep lung deposition of viruses occur i.e. $St_a \leq 0.01$, as shown in Fig. 6e.

3.3.3. Virus Peclet number

Pe_{vi} represents the relative impact of advective muco-ciliary transport and diffusive transport of the viruses in the mucosa (see Eq. 42). The range of Pe_{vi} considered in this study ($4.56 \times 10^7 - 4.56 \times 10^8$) is chosen based on the reported size of SARS-CoV-2 virus [1] and the muco-ciliary clearance rate in a human lung [16].

An increase in Pe_{vi} indicates a larger contribution of muco-ciliary transport (or a smaller impact of diffusion) in the overall transport process and vice-versa. The change in Pe_{vi} considered in this analysis, however, is not observed to cause any significant alterations in virus washout from the lung. This is evident from Fig.7a which shows the virus concentration within the lung for the two extreme Pe_{vi} considered in this analysis, at the end of aerosol exposure ($\tau = 5$) and at $\tau = 10000$. It can be observed that at both time instances the virus concentrations for the two Pe_{vi} overlap each other indicating that the transport rates remain almost invariant. A closer look (see Fig. 7b), however, reveals that the virus concentrations for the two extreme cases differ marginally from each other in the deep lung (beyond $N = 18$) at $\tau = 10000$. The reason for such difference is the relatively faster diffusive transport of the viruses taking place at a lower Pe_{vi} .

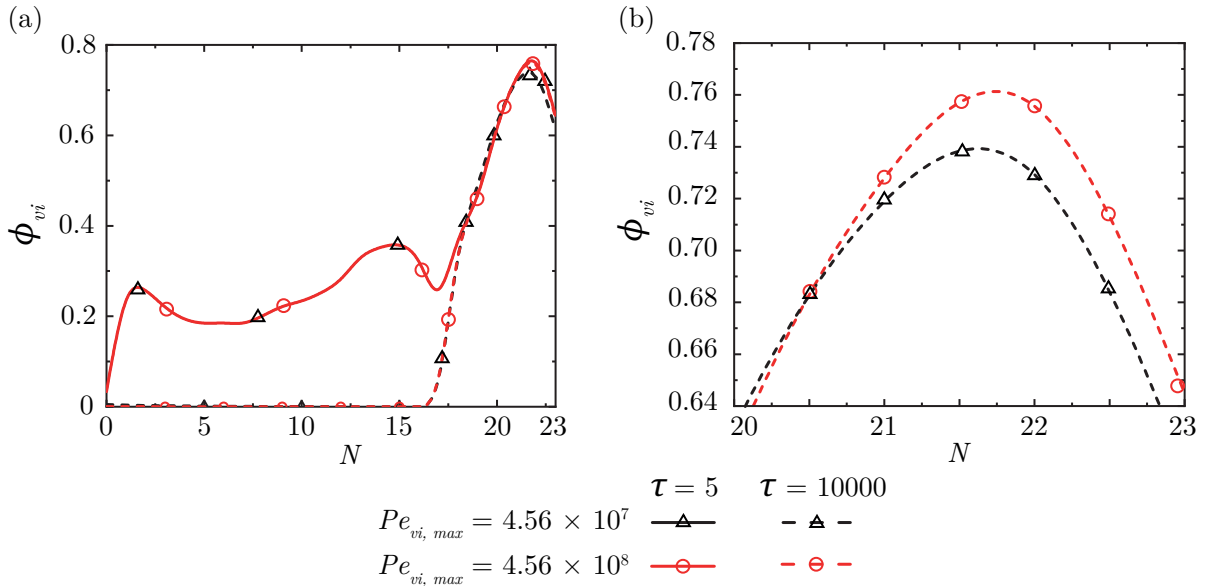


Figure 7: (a) Virus concentration within the lung at the end of exposure ($\tau = 5$) and at $\tau = 10000$ for two different Pe_{vi} . A zoomed view is shown in (b) to clearly illustrate the difference in ϕ_{vi} in the deep lung for the two cases.

3.3.4. Mucus Strouhal number

Strouhal number in the mucus layer (St_m) is defined as the ratio of the time scale of muco-ciliary transport to the breathing time scale (see Eq. 42). A larger St_m , therefore, indicates a longer time scale of muco-ciliary transport, which suggests a slower advective clearance of mucus from the lung and vice-versa. Physiologically, St_m is estimated to vary between 180 and 1440 depending on the breathing time scale, with approximately 360 for a normal breathing time of 4s. Keeping this in mind, the range of St_m variation is considered to be from 100 to 1500 in this analysis.

Figure 8a represents the virus concentration in the mucus layer at the end of aerosol exposure for various St_m . It can be observed that there is no significant difference between the virus concentrations when St_m

remains large. It is only when St_m becomes ~ 100 that deviations become apparent enough. The reason for these deviations is the much faster mucus clearance at low St_m which is able to transport the deposited viruses away from the initial deposition location even before the deposition is complete.

Faster clearance of mucus and hence, washout of viruses from the lung at lower St_m is also evident from the virus concentration within the lung at $\tau = 10000$ and the virus washout curve at $N = 0$ in Figs. 8b, and 8c, respectively. The faster mucus clearance and virus washout is, however, observed to be limited to the upper airways only and does not influence washout of the viruses from the deep lung in any manner (see Fig. 8b). Breathing and muco-ciliary transport are, hence, observed to have no significant influence on virus removal from the deep lung.

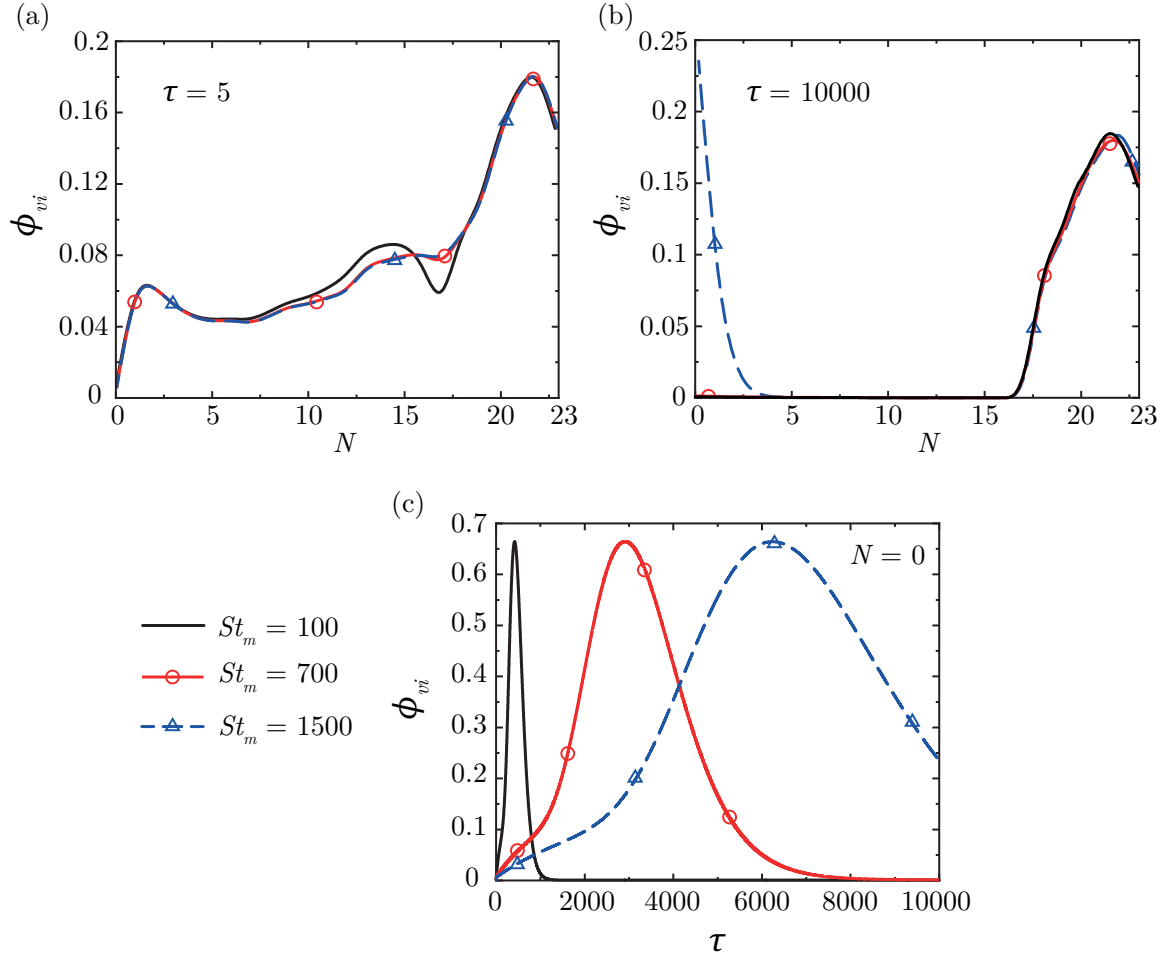


Figure 8: Virus concentration within the lungs for various St_m at (a) the end of aerosol exposure ($\tau = 5$) and (b) at $\tau = 10000$ (c) Temporal change of virus concentration at $N = 0$ for various St_m

3.3.5. Exposure duration

The time duration for which an individual is exposed to the virus-laden aerosols is another important parameter affecting virus transport within the lungs. The impact of exposure duration (τ_{exp}) on virus transport is studied by varying the number of breathing cycles for which the aerosols are inhaled into the lungs.

Figure 9a shows the total amount of aerosols deposited in the airway mucus for various τ_{exp} considered in this analysis. It can be observed that while the deposition pattern within the lungs remain almost identical, the magnitude of deposition increases as τ_{exp} become longer. It is also noted that this increase in deposition magnitude with τ_{exp} has a nearly linear nature, as shown in Fig. 9c.

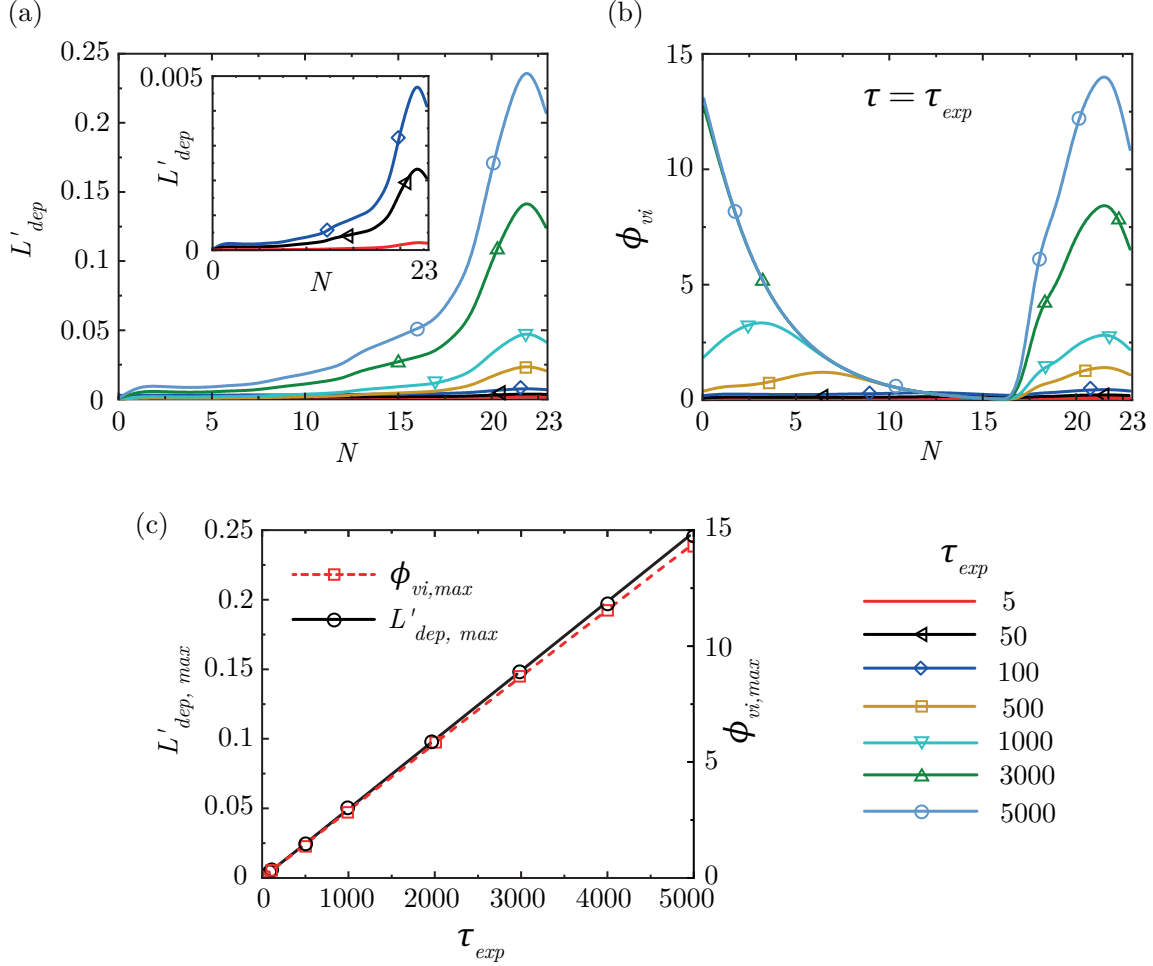


Figure 9: (a) Total aerosol deposition within the lung for different τ_{exp} . Deposition for $\tau_{exp} = 5 - 100$ is additionally shown as inset to ensure proper readability (b) Virus concentration within the lungs for different τ_{exp} at the end of exposure i.e. at $\tau = \tau_{exp}$ (c) Variation in maximum aerosol deposition ($L'_{dep, max}$) and maximum virus concentration ($\phi_{vi, max}$) within the lung with change in τ_{exp}

Figure 9b shows the virus concentration within the lungs for various τ_{exp} at the end of respective exposures. As expected, the virus concentration also increases almost linearly as τ_{exp} becomes longer as a result of the larger aerosol deposition (see Fig. 9c). This is also evident from a comparison of the virus concentrations in the deep lung ($N = 18$ onwards), where advective mucus clearance due to mucociliary transport is absent. In the upper airways (before $N = 18$), mucus advective clearance occurs simultaneously with aerosol deposition and as such, the effective virus concentration is the resultant of virus transport due to the deposition and clearance mechanisms. While virus concentration increases in these generations due to higher aerosol deposition, continuous mucus clearance clears the viruses from these generations towards the 0^{th} generation and as a consequence, the virus accumulates in the first few generations (leading to much higher ϕ_{vi}) before being washed out of the lung.

It can, hence, be concluded that while a larger exposure duration increases viral deposition within the lung, it has no direct influence on virus washout from the lung - which continue to be governed by mucociliary clearance and virus diffusion. However, the larger deposition leads to a longer time requirement for washout of the deposited viruses, which leads to a longer residence time of the viruses within the lung. The larger deposition and longer residence time of viruses increases the probability of the deposited viruses causing infection.

4. Discussion

It is a known fact that clinical complications arise as a result of exposure to respiratory viruses (such as SARS-CoV2). People exposed to such viruses remain asymptomatic or mildly symptomatic in certain cases, while pneumonia-like symptoms and associated complications are also possible. One possible cause for such varied nature of the symptoms is the variability of viral load entering the lungs []. Another probable reason is the location within the respiratory tract location where the viruses are being deposited. It is probable that deep lung depositions of the viruses result in more complicated clinical symptoms, while deposition in the upper airways and the nasopharyngeal region present with more subdued health effects.

Results presented in Section 3 show that viruses deposited before the 18th lung generation is cleared out of the lung at a much faster rate, as compared to viruses that are deposited in the deep lung (18th generation onwards). The primary reason for such difference in the clearance rate is the contribution of muco-ciliary transport, which remains absent after the 18th lung generation. Mucus clearance and hence, virus washout from the lung remains advection-dominated up to the 18th lung generation and diffusion-dominated after 18th lung generation. Since mucus advection is much stronger than virus diffusion in the mucus, the clearance rate is also much faster from the advection-dominated regions. As such, if virus deposition takes place in the deep lung or the viruses somehow reach the deep lung, it will continue to persist in the lung for a very long period of time. The extremely thin respiratory mucosa in the deep lung allows the viruses to come in close contact with the blood vessels surrounding the alveoli. A longer residence time of the viruses in the deep lung, thus, potentially allows the viruses to pass on to the blood stream from the alveoli. This creates a situation by which the viruses can be transported to other parts of the body and infect other organs. Serious and more complicated health issues is a probable outcome of such a situation.

It is, thus, critical to not only understand the conditions under which the viruses can reach the deep lung, but to also explore the means to enhance virus clearance from the lung. These are discussed in the following sections using the results presented in Section 3.

4.1. Virus deposition in the deep lung

The analysis carried out in Section 3 have established that the spatial distribution of virus in the lungs - at the end of exposure - qualitatively follows the aerosol deposition pattern. It is also observed that the main parameters determining the spatial distribution of aerosol deposition in the lungs are $Pe_{ae,max}$, St_a and exposure duration (τ_{exp}). Figure 10 plots the ratio of aerosols deposited in the deep lung to the aerosols deposited in the lung as a function of $Pe_{ae,max}$ and St_a .

A considerable fraction of the virus-laden aerosols ($\sim 50\%$) are observed to be deposited in the deep lung when $Pe_{ae,max}$ remains larger than 2.54×10^7 . This fraction increases to $\sim 75\%$ ($Pe_{ae,max} = 9.65 \times 10^7$) before decreasing to $\sim 13\%$ ($Pe_{ae,max} = 7.18 \times 10^9$). A second increase in the deep lung deposition is observed when $Pe_{ae,max}$ is further increased to 7.18×10^9 ($\sim 50\%$) and then it again decreases to become negligible ($< 1\%$) beyond $Pe_{ae,max} = 3.07 \times 10^{11}$. Deep lung deposition of the aerosols can, thus, be avoided when $Pe_{ae,max}$ remains larger than 3.07×10^{11} or less than 2.37×10^6 . These $Pe_{ae,max}$ values translate to a aerosol droplet size of $10 \mu\text{m}$ and $0.003 \mu\text{m}$, respectively, considering normal breathing in a healthy individual (tidal volume of 1000 ml and a breathing period of 4s). Deep lung deposition can also be minimised if $Pe_{ae,max}$ remains in the range of 4.29×10^9 - 1.6×10^{10} (corresponding aerosol droplet sizes of 0.2 - $0.6 \mu\text{m}$).

It can also be observed from Fig. 10b that deep lung deposition of the aerosols reduce with increase in St_a . As discussed, increase in St_a is possible either when the breathing time scale becomes shorter or the convective time scale becomes longer (inhalation flow velocity becomes smaller). It can, thus, be stated that faster breathing (i.e. shorter breathing time) or shallow breaths can help in reducing deep lung deposition. Similar observations have also been made from experimental investigations carried out by Mallik et al. [27].

It is further observed that exposure duration has a significant influence on deposition of the virus-laden aerosols within the lungs. The amount of deposition increases with exposure duration, which also leads to a longer residence time of the deposited viruses in the lung. Hence, it becomes essential to minimise exposure in order to reduce deposition of viruses in the lung.

4.2. Virus washout from the lung

Once the virus gets deposited within the lung, the most critical aspect is to ensure quick washout of the viruses from the lung. Analysis (see Section 3) have established that virus washout from the lung is

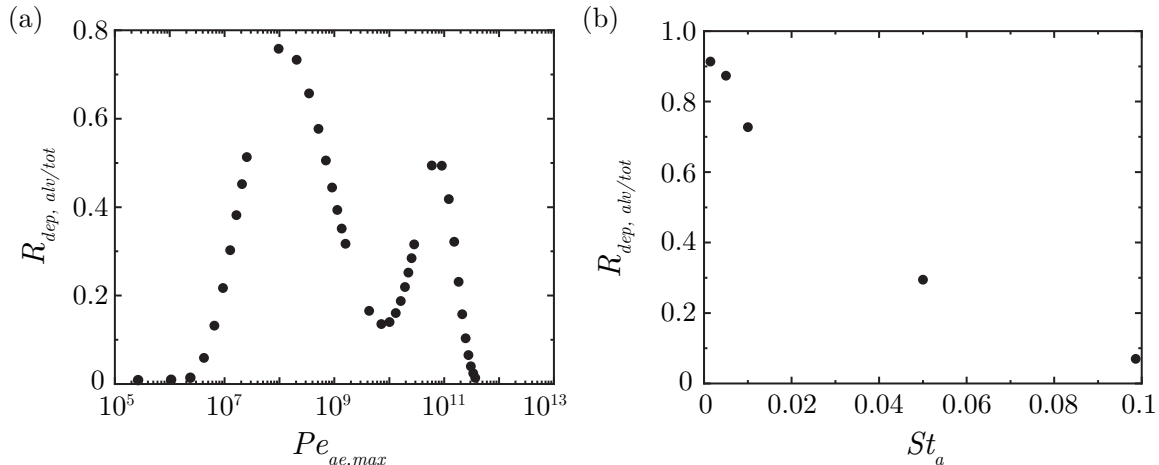


Figure 10: Change in ratio of the aerosols deposited in the deep lung to the total aerosol deposition within the whole lung ($R_{dep, alv/tot}$) with (a) $Pe_{ae,max}$ and (b) St_a

dependent on $Pe_{vi,max}$ and St_m . It is observed that virus washout from the lung is enhanced when both $Pe_{vi,max}$ and St_m decreases, the enhancement with St_m being substantially larger.

Change in Pe_{vi} , keeping all other parameters fixed, suggests a change in diffusivity of virus in the mucus layer (see Section 3.3.3). Virus diffusivity does not influence mucus advection in any form and as such, it is observed that virus clearance from the upper airways (before the 18th generation) remains almost similar with change in Pe_{vi} . Virus clearance in the diffusion-dominated deep lung is, however, observed to become marginally slower when Pe_{vi} increases (i.e. virus diffusivity reduces). It can, thus, be seen that virus diffusivity in the mucus layer plays an important role in determining its clearance from the deep lung. Diffusivity of the virus is determined by its inverse dependence on virus size and viscosity of the mucus layer (see Eq. 42). A smaller virus size and lower viscosity of the mucus layer, as such, promotes faster virus clearance from the lung from the fluid mechanics perspective. While virus size cannot be controlled, mucus property modification is viable and can be a possible approach in enhancing virus clearance from the deep lung.

St_m is observed to mainly influence virus clearance from the advection-dominated region of the lung i.e. before generation 18, while it has no impact on virus clearance from the deep lung. It is observed that an increase in St_m - which indicates longer mucus advection time-scale (smaller advective velocity) or a faster breathing time - impairs virus clearance from the upper airways. A larger mucus advective velocity and a slower breathing process, therefore, promotes virus clearance from the upper airways.

4.3. Migration of deposited viruses

The conditions which promote deep lung deposition of viruses are discussed in Section 4.1. However, it is also possible that viruses that are initially deposited in the upper airways or the throat are transported towards the deep lung at a later time.

Research has revealed that the dominant primary infection site within the human body for SARS-CoV-2 virus is the naso-pharyngeal and the oro-pharyngeal region [1]. Analysis has, however, shown the presence of a significantly higher viral load in sputum samples as compared to throat swabs, especially in symptomatic individuals having moderate to severe health complications. Such observations suggest migration of the deposited viruses from the naso-pharyngeal and the oro-pharyngeal region to the lower respiratory tract. The mechanism of such migration, however, still remains unknown.

One possible mechanism of such migration of the deposited viruses is through aerosolisation of the mucus. The mucus is a highly viscous fluid and as such, does not aerosolise easily. However, in case of imbalance between mucus production in the body and mucus clearance from the body, mucus buildup is possible in the upper airways. One possible cause of imbalance in the mucus clearance is due to irregular ciliary beating - spatially or temporally - or complete impairment of the beating mechanism. Several other factors can also result in these imbalances. The mucus layer can thicken as a result of these imbalances which reduces the

air flow passage in the airways. This promotes aerosolisation of the mucus. The flow passage reduction can also be a result of other clinical issues (such as asthma). In either case, the flow passage constriction can result in air flow blockages in extreme cases and cause violent breakup of the mucus layer. The resulting aerosolised droplets, if they are of the right size, can travel towards and potentially reach the deep lung.

The other mechanism by which the deposited viruses can reach the deep lung is diffusion through the mucus layer itself. This is possible only if the advective mucus clearance is completely absent. Such a situation can be encountered due to complete impairment of the ciliary beating mechanism which controls the muco-ciliary clearance. While this promotes re-aerosolisation of the mucus (as already discussed), it is improbable that the virus will be able to diffuse across the large length required to reach the deep lung. The total length of a typical healthy human lung is ~ 0.28 m, while viruses typically have diffusivity $\sim \mathcal{O}(10^{-13} \text{ m}^2/\text{s})$. However, diffusion through short distances within the lung remains a possibility.

4.4. Estimation of time required for exhibiting influenza-like symptoms from SARS-CoV-2 virus

A survey of available clinical data from individuals infected with SARS-CoV-2 virus show large variability in several parameters of interest. The median incubation period for the SARS-CoV-2 virus has been observed to be 4-5 days after exposure, although it has been observed to extend to as long as 14 days [1]. Samples taken from patients have also revealed that a significant viral load may continue to be present within the human body even after 40 days of exposure, although in most patients the viral load dropped to undetectable levels after 15-20 days [28]. Viral load in symptomatic individuals have been found to vary between $10^2 - 10^7$ (average 10^4) copies/ml in the oro-pharyngeal region, while in sputum samples it has been observed to vary between $10^2 - 10^9$ (average 7×10^6) copies/ml [28, 29]. However, no direct correlation has been observed between the viral load magnitude from the oro-pharyngeal and the sputum samples, except that a higher initial viral load is found in patients who died when compared to recovered patients [28]. Such large variability in data presents considerable difficulty in estimating the time required for exhibiting influenza-like symptoms in an individual infected with the SARS-CoV-2 virus.

The developed mathematical model has been utilised to estimate the time taken for virus concentration within the lung to reach a critical value. The critical concentration is treated as the virus concentration required for an infected individual to exhibit influenza-like symptoms. In order to estimate this time requirement, it is assumed that the respiratory tract is exposed to viruses present in the pharyngeal region, where the SARS-CoV-2 virus initially deposits [1]. Virus concentration at $N = 0$ of the lung model ($c_{vi,0}$) is, thus, assumed to be the clinically observed viral load from oro-pharyngeal samples. The critical concentration within the lung is assumed to be the clinically observed viral load in sputum samples of symptomatic individuals. It is further assumed that the oro-pharyngeal viral load remains constant throughout the exposure duration. It has also been shown in Section 3.3.5 that aerosol deposition and consequently, virus concentration within the lung increases almost linearly with rise in exposure time. The time required for virus concentration within the lung to reach the critical value can, thus, be estimated using linear extrapolation.

It is estimated that the time required for virus concentration within the lung to reach the critical value varies can vary from less than 1 day to approximately 18 days, depending on the viral load in the oro-pharyngeal region. The time-scale estimated using the developed mathematical model is, thus, close to that observed clinically. It has been further observed that the estimated time-scale varies significantly with change in some of the relevant physiological parameters. The variation in time-scale with physiological parameters is shown in Table 3. Only the parameters that show substantial change are mentioned here. It is observed that the time-scale increases substantially when L_0 becomes larger, Q_{max} reduces and T_b becomes shorter, and vice-versa.

Table 3: Variation in estimated time required for exhibiting influenza-like symptoms with change in physiological parameters

Physiological parameter	Change (in %)	Variation in estimated time (in %)
L_0	10	44.16
	-10	-31.66
Q_{max}	10	-29.24
	-10	49.14
T_b	10	-29.13
	-10	49.26

5. Summary

A coupled mathematical model of aerosol and virus transport is developed considering a one-dimensional Weibel-like *trumpet* idealisation of the lung geometry. Virus-laden aerosols are assumed to be inhaled into the lungs for specific exposure durations. The aerosols are transported in the lungs along with the airflow and then deposit in the respiratory mucus through different mechanisms. The deposited viruses are transported within the mucus by a combined action of virus diffusion and muco-ciliary transport. The analysis is carried out in a dimensionless manner and the results are quantified in terms of relevant dimensionless parameters.

It is observed that muco-ciliary transport plays an important role in clearing viruses from the lungs of the deposited viruses. Viruses deposited in the upper respiratory tract (before 18th generation) are washed out relatively faster due to the dominance of muco-ciliary transport, while viruses in the deep lung (after 18th generation) persist for a long time due to absence of mucociliary transport. Longer residence times significantly increase the risk of infection from the viruses. A larger mucus flow rate and a slower breathing is observed to promote virus clearance from the upper respiratory tract. It is further observed that virus clearance from the deep lung can be enhanced only by increasing diffusivity of the viruses in the mucus. This enhancement is, however, marginal. It is, therefore, recommended to take appropriate measures for eliminating situations conducive for deep lung deposition of the viruses. Deep lung deposition of viruses is observed to take place for a specific range of Pe_{ae} . This corresponds to aerosol sizes of 0.003 μm to 10 μm for normal breathing. It is also observed that deep lung deposition is enhanced with slower breathing and deep breaths.

The duration for which the respiratory tract is exposed to the virus-laden aerosols is also observed to have a significant influence on virus washout from the lung. A longer exposure duration is observed to result in larger depositions and consequently, higher virus concentrations in the lungs. As such, a much longer time is needed for virus washout from the lungs leading to longer residence times and greater chances of infection. It is, therefore, recommended to limit the exposure duration as much as possible.

Acknowledgements

The authors gratefully acknowledge the grant provided by MHRD, Govt. of India under the SPARC programme (Project Code: P838).

References

- [1] W. J. Wiersinga, A. Rhodes, A. C. Cheng, S. J. Peacock, H. C. Prescott, Pathophysiology, transmission, diagnosis, and treatment of coronavirus disease 2019 (covid-19): a review, *Jama* 324 (8) (2020) 782–793.
- [2] R. Mittal, R. Ni, J.-H. Seo, The flow physics of covid-19, *Journal of Fluid Mechanics* 894 (2020) F2. doi:10.1017/jfm.2020.330.
- [3] C. Quirouette, N. P. Younis, M. B. Reddy, C. A. Beauchemin, A mathematical model describing the localization and spread of influenza a virus infection within the human respiratory tract, *PLOS Computational Biology* 16 (4) (2020) e1007705.
- [4] A. Guha, Transport and deposition of particles in turbulent and laminar flow, *Annu. Rev. Fluid Mech.* 40 (2008) 311–341.
- [5] W. Hofmann, Modelling inhaled particle deposition in the human lung—a review, *Journal of Aerosol Science* 42 (10) (2011) 693–724.
- [6] A. Chakravarty, N. A. Patankar, M. V. Panchagnula, Aerosol transport in a breathing alveolus, *Physics of Fluids* 31 (12) (2019) 121901.
- [7] R. Fishler, P. Hofemeier, Y. Etzion, Y. Dubowski, J. Sznitman, Particle dynamics and deposition in true-scale pulmonary acinar models, *Scientific reports* 5 (2015) 14071.

- [8] P. Koullapis, P. Hofemeier, J. Sznitman, S. C. Kassinos, An efficient computational fluid-particle dynamics method to predict deposition in a simplified approximation of the deep lung, *European Journal of Pharmaceutical Sciences* 113 (2018) 132–144.
- [9] M. Bailey, E. Ansoborlo, R. Guilmette, F. Paquet, Updating the icrp human respiratory tract model, *Radiation protection dosimetry* 127 (1-4) (2007) 31–34.
- [10] D. B. Taulbee, C. Yu, A theory of aerosol deposition in the human respiratory tract, *Journal of Applied Physiology* 38 (1) (1975) 77–85.
- [11] S. K. Devi, M. V. Panchagnula, M. Alladi, Designing aerosol size distribution to minimize inter-subject variability of alveolar deposition, *Journal of Aerosol Science* 101 (2016) 144–155.
- [12] E. R. Weibel, A. F. Cournand, D. W. Richards, *Morphometry of the human lung*, Vol. 1, Springer, 1963.
- [13] H.-C. Yeh, G. Schum, Models of human lung airways and their application to inhaled particle deposition, *Bulletin of mathematical biology* 42 (3) (1980) 461–480.
- [14] K. Horsfield, G. Cumming, Morphology of the bronchial tree in man., *Journal of applied physiology* 24 (3) (1968) 373–383.
- [15] D. Smith, E. Gaffney, J. Blake, Modelling mucociliary clearance, *Respiratory physiology & neurobiology* 163 (1-3) (2008) 178–188.
- [16] C. Karamaoun, B. Sobac, B. Mauroy, A. Van Muylem, B. Haut, New insights into the mechanisms controlling the bronchial mucus balance, *PloS one* 13 (6) (2018) e0199319.
- [17] A. Handel, L. E. Liao, C. A. Beauchemin, Progress and trends in mathematical modelling of influenza a virus infections, *Current Opinion in Systems Biology* 12 (2018) 30–36.
- [18] A. L. Bauer, C. A. Beauchemin, A. S. Perelson, Agent-based modeling of host–pathogen systems: The successes and challenges, *Information sciences* 179 (10) (2009) 1379–1389.
- [19] M. A. Jensen, Y.-Y. Wang, S. K. Lai, M. G. Forest, S. A. McKinley, Antibody-mediated immobilization of virions in mucus, *Bulletin of mathematical biology* 81 (10) (2019) 4069–4099.
- [20] S. G. K. Devi, *Aerosol deposition studies in human lung - towards personalized medicine*, Ph.D. thesis, IIT Madras, India (2018).
- [21] L. Junqueira, J. Carneiro, R. Kelley, *Basic histology*, 9th edition, Stamford, Conn.: Appleton & Lange, 1998.
- [22] B. Mauroy, C. Fausser, D. Pelca, J. Merckx, P. Flaud, Toward the modeling of mucus draining from the human lung: role of the geometry of the airway tree, *Physical biology* 8 (5) (2011) 056006.
- [23] C. Darquenne, M. Paiva, One-dimensional simulation of aerosol transport and deposition in the human lung, *Journal of applied physiology* 77 (6) (1994) 2889–2898.
- [24] C. Mitsakou, C. Helmis, C. Housiadas, Eulerian modelling of lung deposition with sectional representation of aerosol dynamics, *Journal of Aerosol Science* 36 (1) (2005) 75–94.
- [25] J. Heyder, J. Gebhart, G. Rudolf, C. F. Schiller, W. Stahlhofen, Deposition of particles in the human respiratory tract in the size range 0.005–15 μm , *Journal of aerosol science* 17 (5) (1986) 811–825.
- [26] J.-I. Choi, C. S. Kim, Mathematical analysis of particle deposition in human lungs: an improved single path transport model, *Inhalation toxicology* 19 (11) (2007) 925–939.
- [27] A. K. Mallik, S. Mukherjee, M. V. Panchagnula, An experimental study of respiratory aerosol transport in phantom lung bronchioles, *Physics of Fluids* 32 (11) (2020) 111903.

- [28] J. Fajnzylber, J. Regan, K. Coxen, H. Corry, C. Wong, A. Rosenthal, D. Worrall, F. Giguel, A. Piechocka-Trocha, C. Atyeo, et al., Sars-cov-2 viral load is associated with increased disease severity and mortality, *Nature communications* 11 (1) (2020) 1–9.
- [29] R. Wölfel, V. M. Corman, W. Guggemos, M. Seilmaier, S. Zange, M. A. Müller, D. Niemeyer, T. C. Jones, P. Vollmar, C. Rothe, et al., Virological assessment of hospitalized patients with covid-2019, *Nature* 581 (7809) (2020) 465–469.